5-2023

Light Scattering From Periodic, Conducting Nanostructures

Wesley Kenneth Mills
Utah State University

UtahStateUniversity
MERRILL-CAZIER LIBRARY

LIGHT SCATTERING FROM PERIODIC, CONDUCTING NANOSTRUCTURES

by

Wesley Kenneth Mills

**Capstone submitted in partial fulfillment of
the requirements for graduation with**

University Honors

with a major in
Physics

in the Department of Physics

Approved:

Capstone Mentor	**Departmental Honors Advisor**
Dr. T.-C. Shen	Dr. T.-C. Shen
Committee Member	**University Honors Program Executive Director**
Dr. Mark Riffe	Dr. Kristine Miller

UTAH STATE UNIVERSITY
Logan, UT

Spring 2023

Abstract

A material with broadband light absorbing capabilities has the potential for much usefulness in devices such as photovoltaics and thermoelectrics. By energy conservation, a non-transparent material with low reflectance will be highly absorbing. Thus, much research has been devoted to understanding what makes material having low reflectance across a wide wavelength spectrum.

The importance of a material's electronic structure in determining reflectance is well-established. Current research is revealing the additional importance of surface architecture in the reflective properties of a material. A metasurface is a two-dimentional material with physical features at or smaller than the wavelength of light considered. These wavelength-scale features allow metasurfaces to exhibit uncommon light-matter interactions, such as having a negative index of refraction or generating light beams with orbital angular momentum. Natural or man-made metasurfaces with periodic or quasi-periodic surface features have been found to have extremely low reflectance, but the underlying mechanism has not been clearly established.

Here, mode matching at the boundaries is used to solve a plane wave of light scattering from an array of apertures in a perfectly conducting metal. This approach provides numerical solutions of Maxwell's equations, instead of the commonly used finite-difference-time-domain simulations which provide solutions but can vary with the setup parameters involved in the simulation. My results indicate that interference effects are the primary cause behind the dark nature of periodic metasurfaces. These results provide guidelines to design subwavelength structures that can achieve low reflectance over a broader range of wavelengths.

Furthermore, this technique can be extended to quasi-periodic surfaces. Similar to Fourier analysis, the surface structure could be represented by a distribution of periodic structures where reflectance from each periodic structure can be solved as detailed in this study. These quasi-periodic structures are closer to many ultra-dark surfaces found in nature, such as the dark patches on the wings of some butterfly species. Thus, being able to analyze aperiodic structures could further advance our design of broadband absorbers.

i

Acknowledgements

Without the mentorship of Dr. T.-C. Shen, I never would have gotten to this point in my undergraduate education, so my thanks go out to him first and foremost. I would also like to voice my appreciation for Christian Lange, Dr. Prasad Iyer, Dr. Igal Brener, and Dr. Mark Riffe, who have helped, guided, and taught me all along the way.

The Physics Department at USU has been a great place for me to study and learn to appreciate the discoveries and rigorous analyses made by hundreds of thousands of physicists around the globe in the past millennium. I appreciate all the faculty and administrative staff that I have been blessed to work with while there. The funding I received from the Peak Summer Research Fellowship, the USU Office of Undergraduate Research, and the USU Honors Department has also been a crucial part of making this research possible.

On a more personal note, I want to thank my family, and especially my amazing wife, for their tireless support of my dreams and passions, even when that means having to smile and nod as I explain what a Fourier series is. Your love is deeply appreciated.

Table of Contents

List of Figures

1. Introduction

Humanity has always been fascinated by light. It is, quite literally, how we see the world. Ancient scientists in a few century BC, using glass lenses and bronze mirrors to bend and reflect light, wrote down their observations as some of the foundation of optics. As our understanding has advanced, we have gained greater knowledge of the principles that govern the function of optical devices such as lenses and mirrors. We now understand that the way a material reflects light is primarily a function of (1) the smoothness or roughness of the material's surface and (2) the electronic structures of the material itself.

For the former, consider parallel light rays incident on a perfectly reflecting, perfectly smooth surface as illustrated in Fig. 1(a). Based on the Snell's law of reflection[1] the angle of reflection is equal to the angle of incidence, as measured with respect to the surface normal. Thus, light rays traveling parallel to each other before reflection will continue parallel after reflecting from this surface. Conversely, consider a surface that is perfectly reflecting, but very rough and jagged as illustrated in Fig. 1(b). Parallel incident rays will be scattered in all different directions upon reflection. These two types of reflection are known as specular and diffusive, respectively.
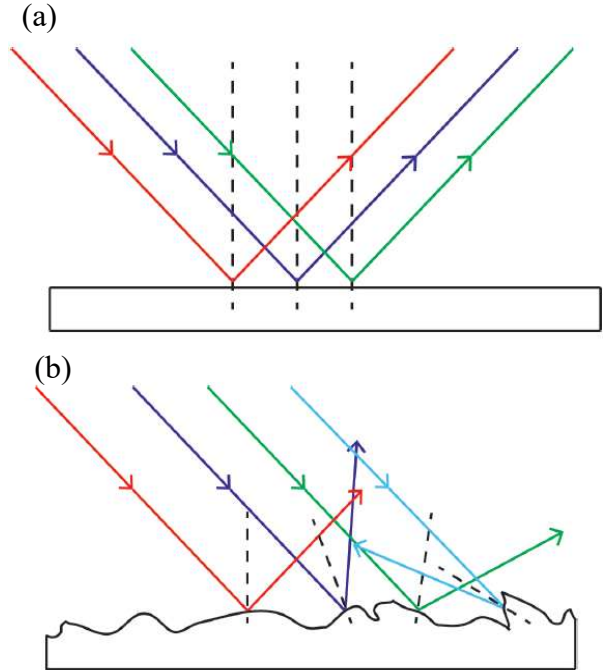
Fig. 1 (a) Specular and (b) diffusive reflection on smooth and rough surfaces, respectively.

The physics of a material's electronic structures are contained within its dielectric function. In a linear, isotropic medium, the dielectric function can be written as

$$\epsilon_r = 1 + \frac{Nq\tilde{x}_0}{\epsilon_0 E_0} \qquad (1)$$

where N is the number of electronic dipoles per unit volume in the material, q is the electron charge, ϵ_o is the vacuum permittivity, E_0 is the amplitude of the driving electric field, and $\tilde{x}_0$ is the complex amplitude of electron oscillation, complex because of the phase difference between the electron displacement and the driving field strength.[2] To get an expression for $\tilde{x}_0$, we can use

the Lorentz models of an electron as a damped, driven oscillator.[3] In this approximation, Newton's second law can be written as

$$\frac{d^2x}{dt^2} + \gamma \frac{dx}{dt} + \omega_0^2 x = \frac{qE_0}{m} \cos(-\omega t) \tag{2}$$

where x is the electron's displacement, γ is the damping coefficient, ω_0 is the resonant frequency of the oscillation, m is the electron mass, and $E_0 \cos(-\omega t)$ is the driving electric field. This differential equation can be solved, and the solution put back into equation 1 to obtain

$$\epsilon_r(\omega) = 1 + \frac{\omega_p^2}{\omega_0^2 - \omega^2 - i\gamma\omega} \tag{3}$$

where $\omega_p^2 = Nq^2/m\epsilon_0$ is known as the plasma frequency of the material. The reflectance of a material, i.e., the fraction of optical power reflected, is in general a function of ϵ_r for the incident and reflecting media.[1] This can get rather complicated, but it will suffice to say that for light incident normally from air onto a material of dielectric coefficient ϵ_r, the reflectance is given by

$$R = \left| \frac{\sqrt{\epsilon_r} - 1}{\sqrt{\epsilon_r} + 1} \right|^2 \tag{4}$$

In air, $\epsilon_r \approx 1$, so the reflectance is approximately 0. This is consistent with our daily experience of light passing through air without reflecting. It is now easy to see that reflectance is, in general, a function of the frequency of the incident light. This makes the choice of material for perfect mirrors nontrivial; you must choose a mirror with a unit reflectance in the wavelength range in which you are working. No material perfectly reflects every wavelength. Figure 2 shows some reflectance spectra of common metals.

As beautiful and useful as mirrors are, modern technology often cares more about the absorptive properties of a material than its reflectance. For example, one possible way to increase the efficiency of a photovoltaic cell, the basic building block of solar energy harvesting, is to design the cell material and structure to have high absorptance over a wider range of wavelengths. Since the sun emits a broad
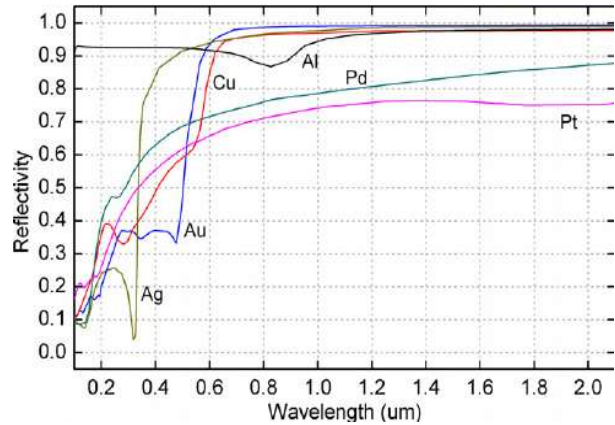

Fig. 2 Reflectance spectra of common metals.[1]
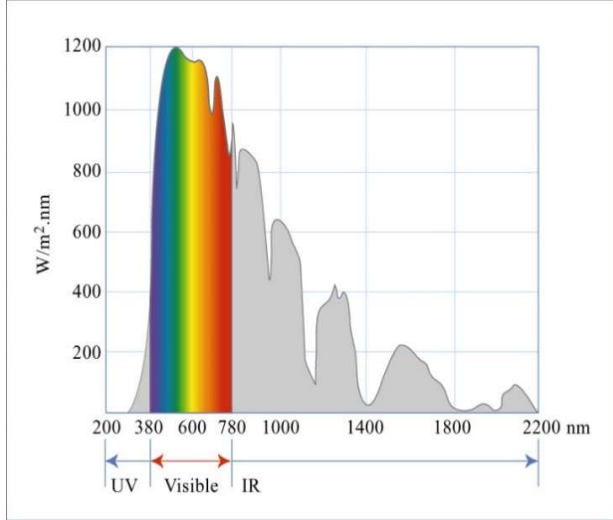
2

Fig. 3 The intensity spectrum emitted by the Sun after passing through the atmosphere. [4]

spectrum, much of the intensity that reaches earth stretches across both the visible and the infrared regimes as depicted in Fig 3.[4] A photovoltaic cell that can efficiently absorb all these wavelengths, a broadband absorber, would be able to produce more electricity from the same amount of incident sunlight. Another type of device, based on the physics of thermoelectrics, can convert a temperature gradient to a voltage or vice versa. The temperature gradient can be generated by thermal radiation from any heat source. These devices can be made more efficiently via a careful selection of the infrared absorption materials and the design of the absorption layer architecture.

Absorption and reflectance are closely related via the principle of energy conservation,

$$R + A + T = 1 \qquad (5)$$

where R is reflectance, A is absorptance, and T is transmittance. All incident energy must be either reflected, absorbed, or transmitted. Just like reflectance, transmittance and absorptance are also functions of the frequency of the incident light. This relation also holds true for matter waves in quantum mechanics. At each interaction of a photon with a material, it has a certain probability of being absorbed. This probability comes from the discrete energy levels the electrons in the material can occupy; a photon of energy $\epsilon = \hbar\omega$ can be absorbed only if the material has one electron at energy state E and one unoccupied state at energy $E + \epsilon$.

Given that photon absorption is a stochastic event, one can see how changing the architecture of the material can enhance light-matter interactions. The more chances a photon can interact with a material, the more likely it can be absorbed at some point during the interaction. The focus of my research is to find an architecture that minimizes reflectance, and thus maximizes absorption, even for a highly reflective bulk material, such as metal. One possible way to enhance photon-material interaction, which has been the subject of much recent investigation, are metamaterials.[5–8] A metamaterial is a structure with features of length scale on the same order of

3

magnitude or smaller than the wavelength of an incident wave. Nature has provided us with some beautiful examples of this effect. The wings and feathers of some insects and birds contain nanostructures that increase light-matter interactions at certain wavelengths and give the animal macroscopic color.[9]
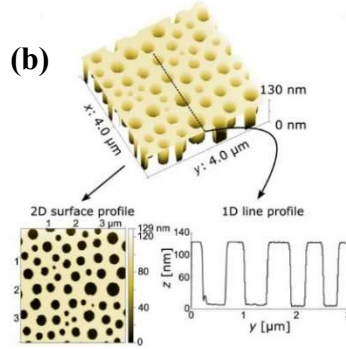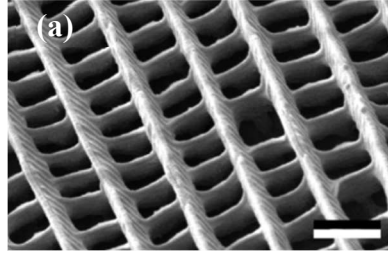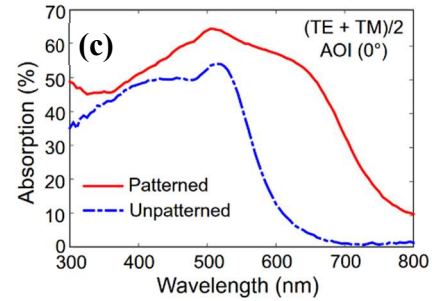

Fig. 4 (a) The nanoscale patterning on the ultradark patches of some butterfly wings.[10] Scale: 1 μm. (b) Patterned thin films of a-Si:H.[11] and (c) absorption spectra of patterned and unpatterned thin films of a:Si:H.[11]

For example, some species of butterflies have nanoscale, cell-like features on their wings that act as an optical metasurface to reduce reflectance to below 1% across nearly the entire visible spectrum as shown in Fig. 4(a).[10] Drawing inspiration from this and similar studies with naturally occurring, optically dark, metamaterials, photovoltaic scientists at Caltech grew bioinspired, randomly patterned, thin films of hydrogenated amorphous silicon (a-Si:H) on glass substrates and measured the absorptance.[11] They found that patterned, thin films of a-Si:H had higher absorptance across a wider range of wavelengths than unpatterned, thin films of the same material [Fig. 4(b)]. These studies provide evidence to the idea that metamaterials can be used to enhance material absorptance and create a broadband absorber.

Another metamaterial that has been explored for creating a broadband absorber is carbon nanotube (CNT) forests. Carbon nanotubes are a quasi-1D (one-dimensional) form of carbon, where the atoms arrange themselves in a tube-like structure with a diameter of ~1 nm and a length can be as long as a few centimeters. When millions of carbon nanotubes are grown vertically and simultaneously on the same substrate, they form what is known as a CNT forest. In addition to growth on a uniform substrate, the morphology of CNT forests can be modulated either randomly as shown in Figs. 5(a) and 5(b)[12,13] or periodically as shown in Fig. 5(c).[14] The modulated CNT forests are among the optically darkest materials known to humankind, with reflectance as low as 0.0002 in the mid-infrared region (Fig. 6).[12] Unfortunately, the optimal design of the forest patterns that is dark across a wide range of wavelengths, from visible to far-IR, has yet to be found.
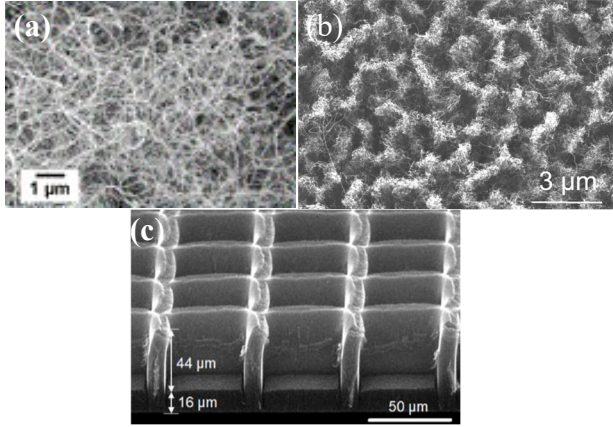
Fig. 5 Top view of CNTs grown on (a) etched aluminum substrate[12], (b) Al/Nb/Si substrate[13], and (c) a catalyst-patterned Si substrate[14].
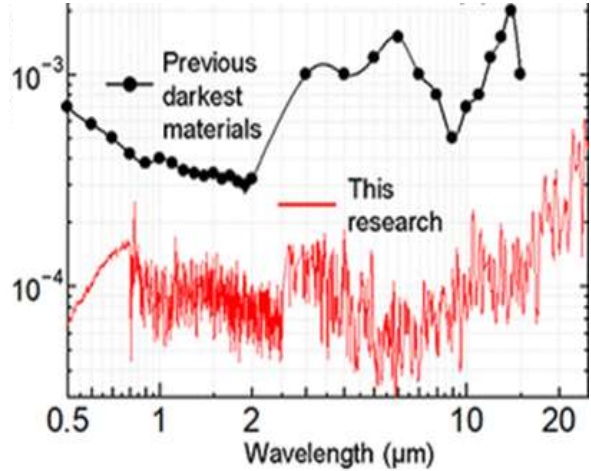

Fig. 6 Reflectance (red) from samples of Fig. 5(a)[12].

The results from these studies of metamaterials indicate that nanometer-structured surfaces could achieve higher absorption than their smooth counterparts and also extend the wavelength range of the absorption to create a broadband absorber. Much theoretical work has been done on this topic using the effective medium approximation, which is valid with dilute, small particles in a medium, like aerosol particles in air, so one can treat the inhomogeneous mixture as an effective homogeneous medium. However, metasurface structures, such as CNT forests, can be of high density and much larger in one dimension than the wavelength scale, invalidating the effective medium approximation. Therefore, Dr. Shen and I decided to study light scattering directly, using Maxwell's equations, for my capstone project. Since CNTs are conductive and distributed randomly on a substrate, the first exercise is to consider an array of semi-infinite metal slabs arranged periodically in the x-direction. When a plane wave of light impinges on the $z = 0$ plane, the symmetry of this array reduces the problem to a two-dimensional (2D) system as illustrated in Fig. 7(a). In this case, the mathematics is simple, because the electric and magnetic field depend only on x and the wave propagation is in the z-direction. After successfully solving the Maxwell equations for this system, the second structure I solved for is an array of semi-infinite rectangular metal tubes, or waveguides. The top view of the interface, $z = 0$, is a metallic grid with rectangular apertures of dimension $a \times b$. [Fig. 7(b)] With the solution of this system, I will explore the various parameters that affect the reflectance of periodic surfaces. I will discuss how my calculation can be extended to describe quasi-periodic surfaces, which may be a more effective way to extend the absorption wavelength range.
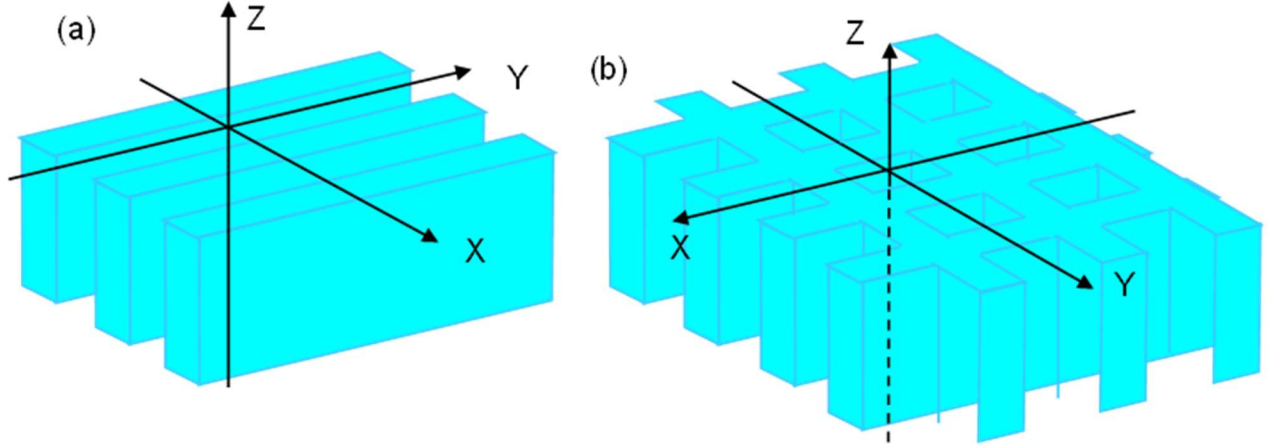
Fig. 7 Schematics of semi-infinite metal slabs with (a) 1D periodicity and (b) 2D periodicity.

2. Floquet theorem and the mode-matching technique

The Floquet theorem[15] is a powerful tool for analyzing wave functions in periodic systems. The theorem states that, in general, the solutions of a periodic system can be written as a linear combination of basis periodic functions. This concept, which is closely related to Fourier theory, has found many uses in mathematics, physics, and engineering. For our purposes, the Floquet theorem means that a light wave propagating in a structure with periodicity L in the x-direction has a x-dependance that can be written as

$$U(x) = \sum_{m=-\infty}^{\infty} A_m e^{-ik_{xm}x} \qquad (6)$$

Similarly, in a 2D system, a light wave propagating in a structure with periodicity L_x in the x-direction and periodicity L_y in the y-direction has x-y dependance that can be expressed as

$$U(x,y) = \sum_{m=-\infty}^{\infty} \sum_{n=-\infty}^{\infty} A_{mn} e^{-ik_{xm}x - ik_{yn}y} \qquad (7)$$

where U might represent the electric field, magnetic field, or a Hertz potential, A_{mn} are the coefficients of the linear combination, and $k_{xm} = k_x + \frac{2\pi m}{L_x}$ and $k_{yn} = k_y + \frac{2\pi n}{L_y}$ are the wavenumbers of the spatial harmonics, with k_x and k_y being the incident wavenumbers in the x and y direction, respectively. I will use the Floquet theorem in my solutions to describe the light scattered by a perfectly conducting structure with x and y periodicity.

6

Mode-matching is a common approach to solving discontinuous boundary problems when the solution on each side of the boundary can be written as a linear combination of orthogonal modes. As an example,[16] consider a metallic waveguide with a discontinuous step in the x direction at $z = 0$ (Fig. 8) and with a TE_{m0} (transverse electric) mode incident on that discontinuity from the $z < 0$ region. The transverse incident fields can be written as
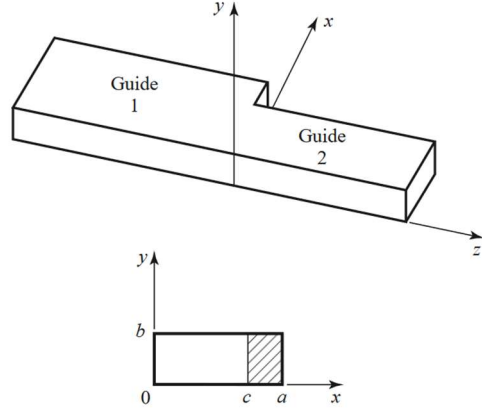
Fig. 8 Rectangular waveguide with discontinuity at $z = 0$.

$$E_{yi} = \sin\left(\frac{m\pi x}{a}\right) e^{-i\beta_m^a z} \tag{7a}$$

$$H_{xi} = -\frac{1}{Z_m^a} \sin\left(\frac{m\pi x}{a}\right) e^{-i\beta_m^a z} \tag{7b}$$

where $\beta_m^a = \sqrt{k^2 - \left(\frac{m\pi}{a}\right)^2}$ and $Z_m^a = \frac{k\eta_0}{\beta_m^a}$ are the propagation constant and impedance of the TE_{m0} mode, respectively, with k being the incident wavenumber and η_0 being the impedance of free space. The discontinuity at $z = 0$ will cause the wave to scatter into infinite TE_{m0} modes, some of which will propagate in the $+z$ and/or $-z$ directions, and many of which will not when m is large enough to make β_m^a imaginary. The modes scattered in the $-z$ direction may be written as

$$E_{yr} = \sum_{n=1}^{\infty} A_n \sin\left(\frac{n\pi x}{a}\right) e^{i\beta_n^a z} \tag{8a}$$

$$H_{xr} = -\sum_{n=1}^{\infty} \frac{A_n}{Z_n^a} \sin\left(\frac{n\pi x}{a}\right) e^{i\beta_n^a z} \tag{8b}$$

while the modes scattered in the $+z$ direction may be written as

$$E_{yt} = \sum_{n=1}^{\infty} B_n \sin\left(\frac{n\pi x}{b}\right) e^{-i\beta_n^b z} \tag{9a}$$

7

$$H_{xt} = -\sum_{n=1}^{\infty} \frac{B_n}{Z_n^b} \sin\left(\frac{n\pi x}{b}\right) e^{-i\beta_n^b z} \qquad (9b)$$

where β_n^b and Z_n^b are the propagation constant and impedance in the $z > 0$ portion of the waveguide.

We can solve for A_n and B_n by applying boundary conditions. We know that each field must be continuous across $z = 0$ in the $x \in (0, b)$ region and that the E_y field must be 0 in the $x \in [b, a]$ region at $z = 0$. Due to a surface current, the H_x field might not be continuous in this region. Thus, we have

$$E_y = \sin\left(\frac{m\pi x}{a}\right) + \sum_{n=1}^{\infty} A_n \sin\left(\frac{n\pi x}{a}\right) = \begin{cases} \sum_{n=1}^{\infty} B_n \sin\left(\frac{n\pi x}{b}\right), & x \in [0, b] \\ 0, & x \in [b, a] \end{cases} \qquad (10a)$$

$$H_x = -\frac{1}{Z_m^a} \sin\left(\frac{m\pi x}{a}\right) - \sum_{n=1}^{\infty} \frac{A_n}{Z_n^a} \sin\left(\frac{n\pi x}{a}\right) = -\sum_{n=1}^{\infty} \frac{B_n}{Z_n^b} \sin\left(\frac{n\pi x}{b}\right), \quad x \in [0, b] \qquad (10b)$$

We now have something in the form of two linear equations for two infinite sets of unknowns, A_n and B_n. Taking advantage of the mutual orthogonality of the sinusoidal functions, we multiply each side of Eq. (10a) by $\sin\left(\frac{\ell\pi x}{a}\right)$ and integrate $\int_0^a dx$, yielding

$$\frac{a}{2} \delta_{m\ell} + \frac{a}{2} A_\ell = \sum_{n=1}^{\infty} B_n \phi_{n\ell} \qquad (11)$$

where $\phi_{n\ell} = \int_0^b \sin\left(\frac{n\pi x}{b}\right) \sin\left(\frac{\ell\pi x}{a}\right) dx$ and $\delta_{m\ell}$ is the Kronecker delta. Similarly, we multiply each side of Eq. (10b) by $\sin\left(\frac{\ell\pi x}{b}\right)$ and integrate $\int_0^b dx$ to get

$$B_\ell = \frac{2Z_\ell^b}{b} \left(\frac{\phi_{\ell m}}{Z_m^a} + \sum_{n=1}^{\infty} \frac{\phi_{\ell n}}{Z_n^a} A_n\right) \qquad (12)$$

We can then substitute this expression for B_ℓ into Eq. (11), after changing the variable of summation to k, and get

8

$$\frac{a}{2}A_\ell - \sum_{n=1}^{\infty}\sum_{k=1}^{\infty}\frac{2\phi_{n\ell}Z_n^b\phi_{nk}}{bZ_k^a}A_k = \sum_{n=1}^{\infty}\frac{2\phi_{n\ell}Z_n^b\phi_{nm}}{bZ_m^a} - \frac{a}{2}\delta_{m\ell} \qquad (13)$$

The values of A_ℓ can be approximated from this equation by truncating the infinite sums to N terms, then rewriting the equation in matrix form so that

$$\overrightarrow{A_\ell} = \left(\frac{a}{2}I_N - V_{\ell k}\right)^{-1}\overrightarrow{P_\ell} \qquad (14)$$

where I_N is the $N \times N$ identity matrix and

$$V_{\ell k} = \sum_{n=1}^{N}\frac{2\phi_{n\ell}Z_n^b\phi_{nk}}{bZ_k^a} \qquad (15a)$$

$$P_\ell = \sum_{n=1}^{N}\frac{2\phi_{n\ell}Z_n^b\phi_{nm}}{bZ_m^a} - \frac{a}{2}\delta_{m\ell} \qquad (15b)$$

Keep in mind that the incident mode is TE$_{m0}$, so in practice m will be known and fixed. Once the A_ℓ are known, the B_ℓ can be found using a truncated Eq. (12). These truncations are known to be valid as long as $N \gg m$, though for many geometries and incident m they are valid as long as N is even a few integers greater than m. It is quite easy to implement this matrix calculation computationally, which is why I have chosen to use this mode-matching technique for my solutions.

Now that we've introduced the basic ideas of the Floquet theorem and mode matching analysis, we can examine light scattering from a perfectly conducting structure that is periodic in 1 direction.

3. Light scattered from one-dimensional periodic structures

Consider an array of metal plates extending infinitely in the y and $z < 0$ directions with periodicity L in the x direction and spacing W as depicted in Fig. (9). For simplicity, I will consider only a light wave of TE polarization
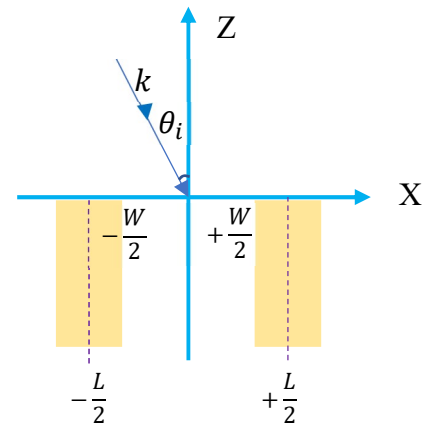

Fig. 9 Semi-infinite metal slabs extending infinitely in the y and $z < 0$ directions and with periodicity L in the x direction and spacing W.

$(\vec{E} = E_y\hat{y})$, incident from $z > 0$ with angle θ, scatters from this structure. The treatment of a TM-polarized wave, where $\vec{H} = H_y\hat{y}$, would follow a similar derivation. For any arbitrary polarization, you can write the wave as a linear combination of a TE and a TM wave, solve individually for each component's scattering, and then recombine linearly to obtain the total scattering results.

The TE incident wave is given by

$$E_{yi} = A_0 e^{-i\beta x + iqz} \tag{16a}$$

$$H_{xi} = \frac{qA_0}{\omega\mu} e^{-i\beta x + iqz} \tag{16b}$$

$$H_{zi} = \frac{\beta A_0}{\omega\mu} e^{-i\beta x + iqz} \tag{16c}$$

where $\beta = k\sin\theta$ and $q = k\cos\theta$ with k being the incident wavenumber. The primary reflected wave is

$$E_{yr} = -A_0 e^{-i\beta x - iqz} \tag{17a}$$

$$H_{xr} = \frac{qA_0}{\omega\mu} e^{-i\beta x - iqz} \tag{17b}$$

$$H_{zr} = \frac{-\beta A_0}{\omega\mu} e^{-i\beta x - iqz} \tag{17c}$$

Using the Floquet theorem, we can write the scattered wave in the $z > 0$ region as

$$E_{ys} = \sum_{n=-\infty}^{\infty} B_n e^{-i\beta_n x - iq_n z} \tag{18a}$$

$$H_{xs} = \frac{-1}{\omega\mu} \sum_{n=-\infty}^{\infty} B_n q_n e^{-i\beta_n x - iq_n z} \tag{18b}$$

$$H_{zs} = \frac{1}{\omega\mu} \sum_{n=-\infty}^{\infty} B_n \beta_n e^{-i\beta_n x - iq_n z} \tag{18c}$$

10

where $\beta_n = \beta + \frac{2\pi n}{L}$ and $q_n = \pm\sqrt{k^2 - \beta_n^2}$. Notice that for a given incident k and θ, there will only be a finite number of values of n such that q_n is real. These are the grating modes which will propagate away from the surface in the $+z$ direction, and for them we choose the positive square root in q_n. The larger n modes, where q_n is imaginary, are surface waves confined to near $z = 0$, which are called evanescent waves. To ensure that the field contribution from these modes becomes negligibly small far away from the $z = 0$ interface, we choose the negative imaginary root.

Since we are assuming the structure to be a perfect conductor, only the TE modes of a parallel plate waveguide will be excited in the $z < 0$ region. Therefore, the transmitted field is of the form

$$E_{yt} = \sum_{n=1}^{\infty} C_n \sin\frac{n\pi\left(x + \frac{W}{2}\right)}{W} e^{ip_n z} \tag{19a}$$

$$H_{xt} = \frac{1}{\omega\mu}\sum_{n=1}^{\infty} C_n p_n \sin\frac{n\pi\left(x + \frac{W}{2}\right)}{W} e^{ip_n z} \tag{19b}$$

$$H_{zt} = \frac{-i}{\omega\mu}\sum_{n=1}^{\infty} \frac{n\pi}{W} C_n \cos\frac{n\pi\left(x + \frac{W}{2}\right)}{W} e^{ip_n z} \tag{19c}$$

where $p_n = \pm\sqrt{k^2 - \left(\frac{n\pi}{W}\right)^2}$. Clearly, for the TE_{n0} mode to propagate down the grating, we must have $k > \frac{n\pi}{W}$. Otherwise, the mode will be confined to near $z = 0$ and we must again choose the negative imaginary root to prevent the field contributions from these surface modes from blowing up at large $|z|$.

Along the $z = 0$ interface, we enforce boundary conditions to solve for B_n and C_n. On the metal region, $|x| \in \left[\frac{W}{2}, \frac{L}{2}\right]$, the transverse electric field and the z component of the magnetic field must be 0. Because of surface currents, this may not be true for the H_x field. In the gap, $|x| < \frac{W}{2}$, all the fields must be continuous. These boundary conditions lead to the set of equations

11

$$E_y = \sum_{n=-\infty}^{\infty} B_n\, e^{-i\beta_n x} = \begin{cases} \displaystyle\sum_{n=1}^{\infty} C_n \sin\frac{n\pi\left(x+\frac{W}{2}\right)}{W}, & |x| < \dfrac{W}{2} \\[4mm] 0, & |x| \in \left[\dfrac{W}{2}, \dfrac{L}{2}\right] \end{cases} \quad (20a)$$

$$H_x = 2qA_0 e^{-i\beta x} - \sum_{n=-\infty}^{\infty} B_n\, q_n e^{-i\beta_n x} = \sum_{n=1}^{\infty} C_n\, p_n \sin\frac{n\pi\left(x+\frac{W}{2}\right)}{W}, \qquad |x| < \dfrac{W}{2} \quad (20b)$$

$$H_z = \sum_{n=-\infty}^{\infty} B_n\, \beta_n e^{-i\beta_n x} = \begin{cases} \displaystyle\sum_{n=1}^{\infty} -i\frac{n\pi}{W} C_n \cos\frac{n\pi\left(x+\frac{W}{2}\right)}{W}, & |x| < \dfrac{W}{2} \\[4mm] 0, & |x| \in \left[\dfrac{W}{2}, \dfrac{L}{2}\right] \end{cases} \quad (20c)$$

We will continue with Eqs. (20a) and (20b), but after finding B_n and C_n one can show that Eq. (20c) is automatically satisfied.

Multiply both sides of Eq. (20a) by $e^{i\beta_m x}$ and integrate $\int_{-L/2}^{L/2} dx$. Then multiple both sides of Eq. (20b) by $\sin\frac{m\pi\left(x+\frac{W}{2}\right)}{W}$ and integrate $\int_{-W/2}^{W/2} dx$. This will lead to

$$B_m L = \sum_{n=1}^{\infty} C_n\, \phi_{mn}^+ \qquad (21a)$$

$$C_m = \frac{2}{W p_m}\left(2qA_0 \phi_{0m}^- - \sum_{n=-\infty}^{\infty} B_n q_n\, \phi_{nm}^- \right) \qquad (21b)$$

where $\phi_{mn}^{\pm} = \int_{-W/2}^{W/2} e^{\pm i\beta_m x} \sin\left(\frac{n\pi}{W}\left(x+\frac{W}{2}\right)\right) dx$. These equations can easily be solved numerically, as discussed in Sec. 2. Substitute Eq. (21b) into Eq. (21a), truncate the infinite sums to N terms such that $n \in [1, N]$ in Eq. (21a) and $n \in \left[-\frac{N-1}{2}, \frac{N-1}{2}\right]$ in Eq. (21b), and rewrite the problem as a matrix equation with unknown vector $\overrightarrow{B_m}$. Once B_n is known, use Eq. (21b) to obtain C_n. An appropriate N can be found by trial and error, ensuring that the resultant B_n and C_n satisfy Eqs. (20a)-(20c). In my implementation, I found that $N = 19$ was adequate for $W = 700$ nm, $L = 1000$ nm, $\lambda_0 = 343$ nm, and any incident angle.

Once the coefficients are known, the incident, reflected, and transmitted power in the z direction can be calculated as

$$|P_{zi}| = \frac{-1}{2} \Re e [E_{yi} \times H_{xi}^*] = \frac{q}{2\omega\mu} |A_0|^2 \qquad (22\text{a})$$

$$|P_{zr}| = \frac{-1}{2L} \Re e \left[\int_{-L/2}^{L/2} [(E_{yr} + E_{ys}) \times (H_{xr}^* + H_{xs}^*)] \, dx \right]$$

$$= \frac{q}{2\omega\mu} [|A_0 - B_0|^2 + \sum_{\substack{n=-(N-1)/2 \\ n \neq 0}}^{(N-1)/2} \frac{\Re e[q_n]}{2\omega\mu} |B_n|^2 \qquad (22\text{b})$$

$$|P_{zt}| = \frac{1}{2L} \Re e \left[\int_{-L/2}^{L/2} [E_{yt} \times H_{xt}^*] \, dx \right] = \frac{W}{4L} \sum_{n=1}^{N-1} \frac{\Re e[p_n]}{\omega\mu} |C_n|^2 \qquad (22\text{c})$$

In the sums, only propagating modes, where q_n or p_n are real, will contribute to the reflected or transmitted power. The modes for which q_n or p_n are imaginary will not carry away any power; instead the power in these modes will be stored in surface currents along the $z = 0$ interface. Thus, the complete power conservation equation can be written as

$$|P_{zi}| = |P_{zr}| + |P_{zt}| + |P_{zs}| \qquad (23)$$

where $|P_{zs}|$ is the stored power.

3.1 One-dimensional results

I conducted this calculation in MATLAB. An example result is shown in Fig. (10). Reflectance and transmittance are defined as $R = |P_{zr}|/|P_{zi}|$ and $T = |P_{zt}|/|P_{zi}|$, respectively. The stored power is negligible, $R + T \approx 1$, for all wavelengths. For simplicity, I will only show reflectance results from now on.

At $\lambda = 2W$, the structure becomes totally reflective. This is a direct result of the cutoff
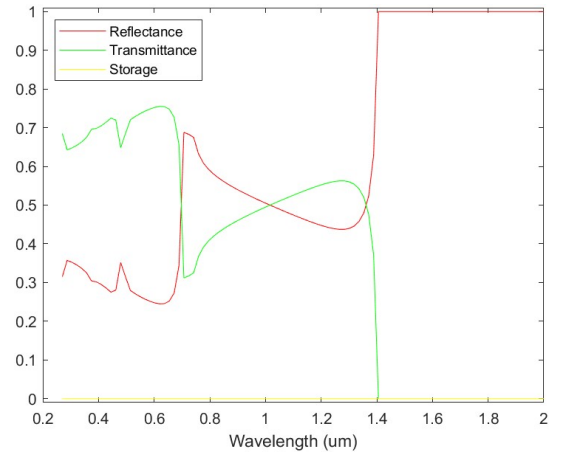

Fig. 10 Results of 1D calculation for $W = 0.7$ μm, L= 1.0 μm, $\theta = 30°$. In all my results, $R + T \approx 1$ across the spectrum.

wavelength of a parallel-plate waveguide, which is $2W$. Light with a longer wavelength cannot propagate in the waveguide region ($z < 0$), so it will be reflected entirely.

Moving towards shorter wavelengths, the reflectance drops quickly then begins to oscillate. These oscillations are caused by interference between scattered waves. Basic interference theory tells us that far-field intensity oscillations, or fringes, due to interference from point sources are strongest when $\lambda \lesssim d$, where d is the source spacing. This is the exact result we see for metal slabs with various periodicities, L as shown in Fig. (11). We can thus deduce that these oscillations are due to interference.

In the shortest wavelength, the reflectance approaches the geometric limit, i.e., the ratio of metal to gap at the interface, $\frac{1-W}{L}$. The geometric limits are marked in Figure 12. Indeed, the $\lambda \to 0$ limit is valid for geometric optics, so we expect that the reflectance should approach such a value in this limit.

All these results vindicate the mode-match assumption used for describing light scattering from a 1D, perfectly conducting, periodic structure. Next, we will extend this model to describe a surface of 2D periodicity.
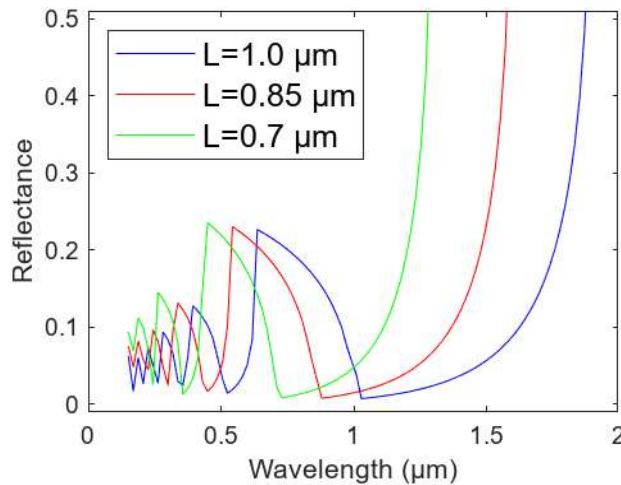
Fig. 11 Results of 1D calculation with metal thickness $L - W = 0.05$ μm and $\theta = 1°$.
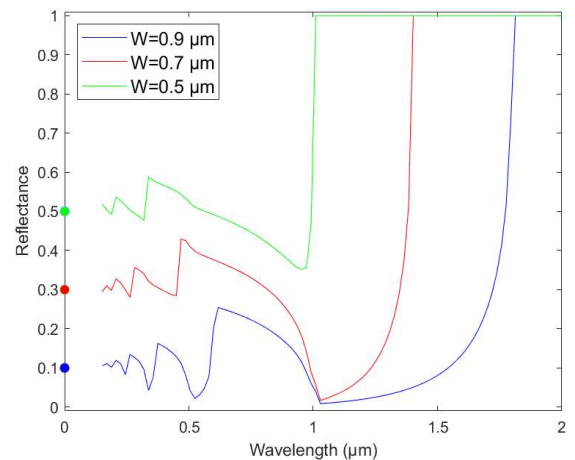
Fig. 12 Results of 1D calculation with $L = 1.0$ μm and $\theta = 1°$. The geometric limit of each calculation is marked on the y axis.

4. Light scattered from two-dimensional periodic structures

For the 2D case, consider a perfect metal structure with a periodic array of rectangular holes extending infinitely in the x-y plane and semi-infinitely in $z < 0$. Light is incident on the structure from $z > 0$ with polar angle θ and azimuthal angle ϕ as illustrated in Fig. 13. We will

14

Fig. 13 Setup for 2D case. The $z > 0$ region is free space. The blue regions in $z < 0$ are waveguides and the white regions are a perfectly conducting metal.

once again consider a TE incident wave, where $\vec{E} = E_x \hat{x} + E_y \hat{y}$, but a similar analysis can be performed for a TM wave, where $\vec{H} = H_x \hat{x} + H_y \hat{y}$. The results of any arbitrary polarization can then be built as a linear combination of the two.

The TE incident wave is given by

$$E_{xi} = \sin\phi \, A_0 e^{-ik_x x - ik_y y + ik_z z} \tag{24a}$$

$$E_{yi} = -\cos\phi \, A_0 e^{-ik_x x - ik_y y + ik_z z} \tag{24b}$$
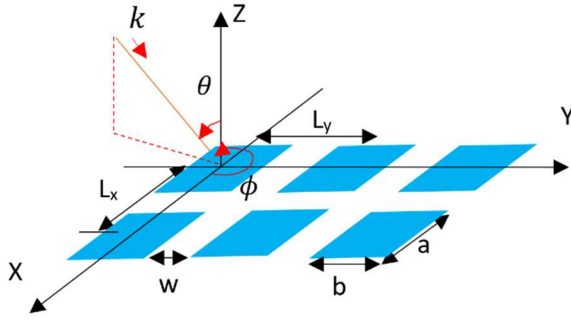
$$H_{xi} = -\cos\theta \cos\phi \, \frac{A_0}{\eta} e^{-ik_x x - ik_y y + ik_z z} \tag{24c}$$

$$H_{yi} = -\cos\theta \sin\phi \, \frac{A_0}{\eta} e^{-ik_x x - ik_y y + ik_z z} \tag{24d}$$

$$H_{zi} = +\sin\theta \, \frac{A_0}{\eta} e^{-ik_x x - ik_y y + ik_z z} \tag{24e}$$

where $k_x = -k \sin\theta \cos\phi$, $k_y = -k \sin\theta \sin\phi$, and $k_z = k \cos\theta$ and $\eta = \sqrt{\mu/\epsilon}$ is the impedance of the medium. The primary reflected wave is

$$E_{xr} = -\sin\phi \, A_0 e^{-ik_x x - ik_y y - ik_z z} \tag{25a}$$

$$E_{yr} = \cos\phi \, A_0 e^{-ik_x x - ik y - ik_z z} \tag{25b}$$

$$H_{xr} = -\cos\theta \cos\phi \, \frac{A_0}{\eta} e^{-ik_x x - ik_y y - ik_z z} \tag{25c}$$

15

$$H_{yr} = -\cos\theta \sin\phi \frac{A_0}{\eta} e^{-ik_x x - ik_y y - ik_z z} \qquad (25\text{d})$$

$$H_{zr} = -\sin\theta \frac{A_0}{\eta} e^{-ik_x x - ik_y y - ik_z z} \qquad (25\text{e})$$

Using the 2D Floquet theorem discussed in Sec. 2, we can write the scattered wave in the $z > 0$ region as

$$E_{xs} = \sum_{m,n=-\infty}^{\infty} B_{mn} \, e^{-ik_{xm}x - ik_{yn}y - iq_{mn}z} \qquad (26\text{a})$$

$$E_{ys} = \sum_{m,n=-\infty}^{\infty} C_{mn} \, e^{-ik_{xm}x - ik_{yn}y - iq_{mn}z} \qquad (26\text{b})$$

$$H_{xs} = \frac{-1}{\omega\mu} \sum_{m,n=-\infty}^{\infty} q_{mn} \, C_{mn} e^{-ik_{xm}x - ik_{yn}y - iq_{mn}z} \qquad (26\text{c})$$

$$H_{ys} = \frac{1}{\omega\mu} \sum_{m,n=-\infty}^{\infty} q_{mn} B_{mn} \, e^{-ik_{xm}x - ik_{yn}y - iq_{mn}z} \qquad (26\text{d})$$

$$H_{zs} = \frac{1}{\omega\mu} \sum_{m,n=-\infty}^{\infty} \left(k_{xm} C_{mn} - k_{yn} B_{mn} \right) e^{-ik_{xm}x - ik_{yn}y - iq_{mn}z} \qquad (26\text{e})$$

where $k_{xm} = k_x + \frac{2\pi m}{L_x}$, $k_{yn} = k_y + \frac{2\pi n}{L_y}$, and $q_{mn} = \pm\sqrt{k^2 - k_{xm}^2 - k_{yn}^2}$. For m, n such that q_{mn} is imaginary, we once again choose the negative square root to ensure that those modes die off far away from $z = 0$. The H fields are obtained from the Maxwell relations

$$H_x = \frac{i}{\omega\mu} \left(\partial_y E_z - \partial_z E_y \right) = \frac{-i}{\omega\mu} \partial_z E_y \qquad (27\text{a})$$

$$H_y = \frac{i}{\omega\mu} \left(\partial_z E_x - \partial_x E_z \right) = \frac{i}{\omega\mu} \partial_z E_x \qquad (27\text{b})$$

$$H_z = \frac{i}{\omega\mu}\left(\partial_x E_y - \partial_y E_x\right) \qquad (27c)$$

In the $z < 0$ region, the waves will take the form of TE modes propagating in a perfectly conducting, rectangular waveguide.

$$E_{xt} = \frac{i\omega\mu\pi}{b}\sum_{\substack{r,s=0\\(r,s)\neq(0,0)}}^{\infty}\frac{sD_{rs}}{K_{rs}^2}\cos\frac{r\pi(x+a/2)}{a}\sin\frac{s\pi(y+b/2)}{b}e^{ip_{rs}z} \qquad (28a)$$

$$E_{yt} = \frac{-i\omega\mu\pi}{a}\sum_{\substack{r,s=0\\(r,s)\neq(0,0)}}^{\infty}\frac{rD_{rs}}{K_{rs}^2}\sin\frac{r\pi(x+a/2)}{a}\cos\frac{s\pi(y+b/2)}{b}e^{ip_{rs}z} \qquad (28b)$$

$$H_{xt} = \frac{-i\pi}{a}\sum_{\substack{r,s=0\\(r,s)\neq(0,0)}}^{\infty}\frac{rp_{rs}D_{rs}}{K_{rs}^2}\sin\frac{r\pi(x+a/2)}{a}\cos\frac{s\pi(y+b/2)}{b}e^{ip_{rs}z} \qquad (28c)$$

$$H_{yt} = \frac{-i\pi}{b}\sum_{\substack{r,s=0\\(r,s)\neq(0,0)}}^{\infty}\frac{sp_{rs}D_{rs}}{K_{rs}^2}\cos\frac{r\pi(x+a/2)}{a}\sin\frac{s\pi(y+b/2)}{b}e^{ip_{rs}z} \qquad (28d)$$

$$H_{zt} = \sum_{\substack{r,s=0\\(r,s)\neq(0,0)}}^{\infty}D_{rs}\cos\frac{r\pi(x+a/2)}{a}\cos\frac{s\pi(y+b/2)}{b}e^{ip_{rs}z} \qquad (28e)$$

where $p_{rs} = \pm\sqrt{k^2 - K_{rs}^2}$ and $K_{rs} = \sqrt{\left(\frac{r\pi}{a}\right)^2 + \left(\frac{s\pi}{b}\right)^2}$. As discussed before, the negative imaginary root of p_{rs} should be taken. Notice that these equations still follow the Maxwell's relations of Eqs. (27a) - (27c) in addition to the relations

$$E_x = \frac{-i}{\omega\epsilon}\left(\partial_y H_z - \partial_z H_y\right) \qquad (29a)$$

$$E_y = \frac{-i}{\omega\epsilon}\left(\partial_z H_x - \partial_x H_z\right) \qquad (29b)$$

17

Applying boundary conditions at $z = 0$, similar to the 1D case, we get two pairs of equations that we can use to solve for B_{mn}, C_{mn}, and D_{rs}, as well as a fifth equation we can use to check the validity of our solution. The first pair of equations come from the E_y and H_x boundary conditions.

$$E_y = \sum_{m,n=-\infty}^{\infty} C_{mn} e^{-ik_{xm}x-ik_{yn}y}$$

$$= \begin{cases} \dfrac{-i\omega\mu\pi}{a} \displaystyle\sum_{\substack{r,s=0 \\ (r,s)\neq(0,0)}}^{\infty} \dfrac{rD_{rs}}{K_{rs}^2} \sin\dfrac{r\pi(x+a/2)}{a} \cos\dfrac{s\pi(y+b/2)}{b}, & \text{gap} \\ \\ 0, & \text{metal} \end{cases} \quad (30a)$$

$$H_x = -2\cos\theta\cos\phi\, \dfrac{A_0}{\eta} e^{-ik_x x-ik_y y} - \dfrac{1}{\omega\mu} \sum_{m,n=-\infty}^{\infty} q_{mn} C_{mn} e^{-ik_{xm}x-ik_{yn}y}$$

$$= \dfrac{-i\pi}{a} \displaystyle\sum_{\substack{r,s=0 \\ (r,s)\neq(0,0)}}^{\infty} \dfrac{rp_{rs}D_{rs}}{K_{rs}^2} \sin\dfrac{r\pi(x+a/2)}{a} \cos\dfrac{s\pi(y+b/2)}{b}, \qquad \text{gap} \quad (30b)$$

Here, "gap" denotes the region $|x| < \frac{a}{2}, |y| < \frac{b}{2}$, while "metal" denotes the portion of $|x| < \frac{L_x}{2}, |y| < \frac{L_y}{2}$ that is not in the gap. The second pair of equations come from the E_x and H_y boundary conditions.

$$E_x = \sum_{m,n=-\infty}^{\infty} B_{mn} e^{-ik_{xm}x-ik_{yn}y}$$

$$= \begin{cases} \dfrac{i\omega\mu\pi}{b} \displaystyle\sum_{\substack{r,s=0 \\ (r,s)\neq(0,0)}}^{\infty} \dfrac{sD_{rs}}{K_{rs}^2} \cos\dfrac{r\pi(x+a/2)}{a} \sin\dfrac{s\pi(y+b/2)}{b}, & \text{gap} \\ \\ 0, & \text{metal} \end{cases} \quad (31a)$$

$$H_y = -2\cos\theta\sin\phi\,\frac{A_0}{\eta}e^{-ik_xx-ik_yy} + \frac{1}{\omega\mu}\sum_{m,n=-\infty}^{\infty}q_{mn}B_{mn}\,e^{-ik_{xm}x-ik_{yn}y}$$

$$= \frac{-i\pi}{b}\sum_{\substack{r,s=0\\(r,s)\neq(0,0)}}^{\infty}\frac{sp_{rs}D_{rs}}{K_{rs}^2}\cos\frac{r\pi(x+a/2)}{a}\sin\frac{s\pi(y+b/2)}{b}, \qquad \text{gap} \qquad (\,31b\,)$$

The fifth equation, which describes the H_z field boundary condition, can be used to verify the validity of a B_{mn}, C_{mn}, D_{rs} solution.

$$H_z = \frac{1}{\omega\mu}\sum_{m,n=-\infty}^{\infty}\left(k_{xm}C_{mn} - k_{yn}B_{mn}\right)e^{-ik_{xm}x-ik_{yn}y}$$

$$= \begin{cases} \displaystyle\sum_{\substack{r,s=0\\(r,s)\neq(0,0)}}^{\infty}D_{rs}\cos\frac{r\pi(x+a/2)}{a}\cos\frac{s\pi(y+b/2)}{b}, & \text{gap} \\[1em] 0, & \text{metal} \end{cases} \qquad (\,32\,)$$

Taking advantage of the orthogonality of sines, cosines, and complex exponentials, similar to what was done in the 1D case, we can transform the first pair of equations, Eqs. (30a) and (30b), into the relation

$$C_{mn} = \frac{-i\omega\mu\pi}{aL_xL_y}\sum_{r=1}^{\infty}\sum_{s=0}^{\infty}\frac{rD_{rs}}{K_{rs}^2}\psi_{mr}^+(a)\phi_{ns}^+(b) \qquad (\,33a\,)$$

$$D_{rs} = \frac{-i4K_{rs}^2}{\pi brp_{rs}(1+\delta_{s0})}\left(2\cos\theta\cos\phi\,\frac{A_0}{\eta}\psi_{0r}^-(a)\phi_{0s}^-(b)\right.$$
$$\left.+\frac{1}{\omega\mu}\sum_{m,n=-\infty}^{\infty}q_{mn}C_{mn}\psi_{mr}^-(a)\phi_{ns}^-(b)\right) \qquad (\,33b\,)$$

where $\psi_{mr}^\pm = \int_{-a/2}^{a/2}e^{\pm ik_{xm}x}\sin\left(\frac{r\pi}{a}\left(x+\frac{a}{2}\right)\right)dx$ and $\phi_{ns}^\pm = \int_{-b/2}^{b/2}e^{\pm ik_{yn}y}\cos\left(\frac{s\pi}{b}\left(y+\frac{b}{2}\right)\right)dy$.
To solve this system, plug Eq. (33b) into Eq. (33a), appropriately truncate the infinite sum, and rewrite it as a matrix equation that can be solved for $\overrightarrow{C_{mn}}$. All of D_{rs} excluding D_{0s}, can then be found from Eq. (\,33b).

A similar procedure can be followed for the other pair of Eqs (31)a and (31b), to find B_{mn} and D_{rs} excluding D_{r0}. Use Eq. (32) to check the validity of the solution.

Once the coefficients are all known, the incident, reflected, and transmitted power can be calculated using

$$|P_{zi}| = \frac{-1}{2L_xL_y} \Re e \left[\int_{-L_x/2}^{L_x/2} dx \int_{-L_y/2}^{L_y/2} dy \left[E_{xi} \cdot H_{yi}^* - E_{yi} \cdot H_{xi}^* \right] \right] = \frac{|A_0|^2}{2\eta} \cos\theta \quad (34a)$$

$$|P_{zr}| = \frac{1}{2L_xL_y} \Re e \left[\int_{-L_y/2}^{L_y/2} dy \int_{-L_x/2}^{L_x/2} dx \left[(E_{xr} + E_{xs}) \cdot (H_{yr}^* + H_{ys}^*) \right. \right.$$

$$\left. \left. - (E_{yr} + E_{ys}) \cdot (H_{xr}^* + H_{xs}^*) \right] \right]$$

$$= \frac{1}{2} \left[\frac{|A_0|^2}{\eta} \cos\theta + \frac{1}{\omega\mu} \sum_{m,n=-(N-1)/2}^{(N-1)/2} (|B_{mn}|^2 + |C_{mn}|^2) \cdot \overline{q_{mn}} \right.$$

$$\left. + \frac{2\overline{A_0} \cos\theta}{\eta} (\cos\phi \, \overline{C_{00}} - \sin\phi \, \overline{B_{00}}) \right]$$

$$(34b)$$

$$|P_{zt}| = \frac{-1}{2L_xL_y} \Re e \left[\int_{-b/2}^{b/2} dy \int_{-a/2}^{a/2} dx \left[E_{xt} \cdot H_{yt}^* - E_{yt} \cdot H_{xt}^* \right] \right]$$

$$= \frac{ab\omega\mu}{8L_xL_y} \sum_{\substack{r,s=0 \\ (r,s)\neq(0,0)}}^{\infty} \frac{\overline{p_{rs}} \, |D_{rs}|^2}{K_{rs}^4} \left(\left(\frac{s\pi}{b}\right)^2 (1 + \delta_{r0}) + \left(\frac{r\pi}{a}\right)^2 (1 + \delta_{s0}) \right)$$

$$(34c)$$

where the bar denotes the real part. As in Sec. 3.1, the stored power is negligible.

4.1 Two-dimensional results

Typically, reflectance is measured at normal incidence. Due to numerical issues at $\theta = 0°$, results were calculated using $\theta = 1°$, unless otherwise specified. Assuming that the solution is stable, normal incidence would produce approximately the same spectrum results.

The cutoff wavelength for a rectangular waveguide is $\lambda = 2a$, where a is the longest dimension of the rectangular cross-section. The geometric ratio of metal per unit cell for this 2D geometry is $1 - \frac{ab}{L_xL_y}$. Both of these ideas are consistent with my 2D solutions, as shown in Fig. 14. There are strong oscillations in the reflectance spectra at $\lambda \lesssim L$ (Fig. 15), indicative of interference between the scattered waves, as we saw in the 1D solutions.
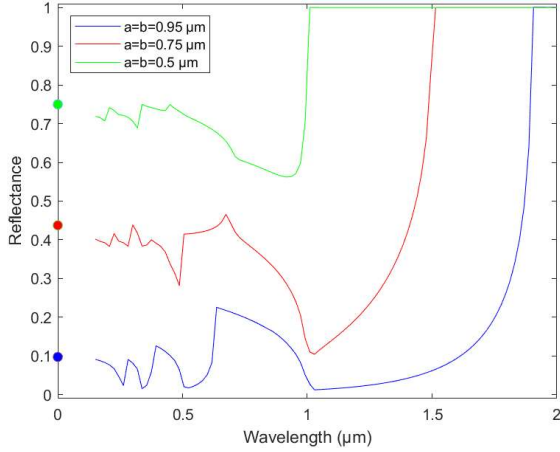
20

Fig. 14 Results of 2D calculation with $L_x = L_y = 1.0$ μm and $\phi = 45°$. The geometric limit of each calculation is marked on the y axis.
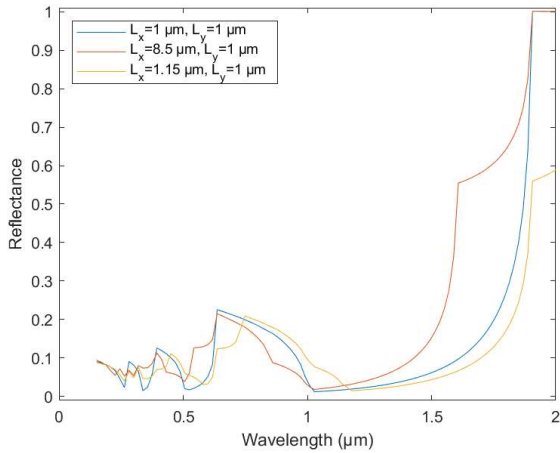

Fig. 15 Results of 2D calculation with metal thickness 0.05 μm and $\phi = 45°$. Just as in the 1D case, reflectance begins to oscillate when $\lambda = L_x$ or L_y, whichever is greater. A secondary oscillation begins when the wavelength equals the smaller of the two periodicities.

In all these results, we see that reflectance depends heavily on the wavelength of light in question. This phenomenon is also responsible for "structural color", found in the feather barbules of the bird of paradise and other bird and insect species.[9] Since we are considering a bulk material that reflects all colors perfectly, like the long wavelength limit of Fig. 2, the wavelength dependence of color must be due to the physical structure of the material. The results of my solution illustrate that structural color is largely an interference effect.

In the basic case of specular reflectance from a flat interface, reflectance increases with θ. We would expect a similar result from this calculation, and indeed reflectance does increase with incident polar angle, as shown in Fig. 16. Changing the incident azimuthal angle affects the way that the incident light couples into the transmitted waveguide modes (Fig. 17). Interestingly, $\phi = 0°$ and $\phi = 45°$ incidence produce nearly the same reflectance spectrum, while $\phi = 30°$ has higher overall reflectance. The $\phi = 0°$ case is particularly interesting, because this is a similar system to the 1D-periodicity calculation. The electric field is entirely in the y-direction, but rather than an uninterrupted aperture in that same direction for $z < 0$, as in the 1D-periodic case, the transmitted wave is now broken up by periodic metal plates. This changes the allowed modes that can be transmitted, but for thin enough plates the reflectance results are very similar to the 1D case (Sec. 4.2).
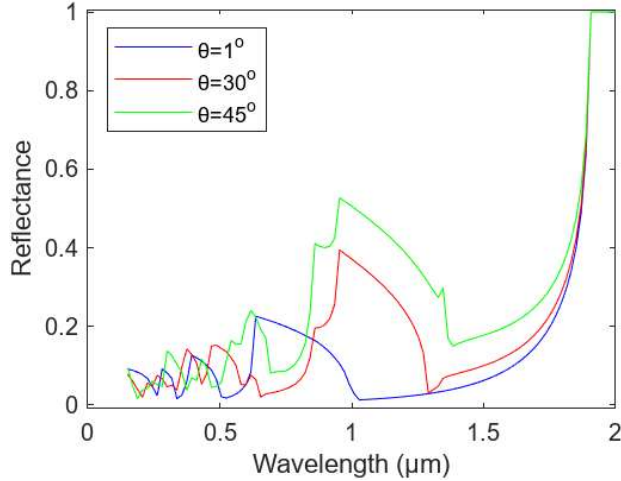
21

Fig. 16 Results of 2D calculation with $a = b = 0.95$ μm, $L_x = L_y = 1.0$ μm, and $\phi = 45°$.
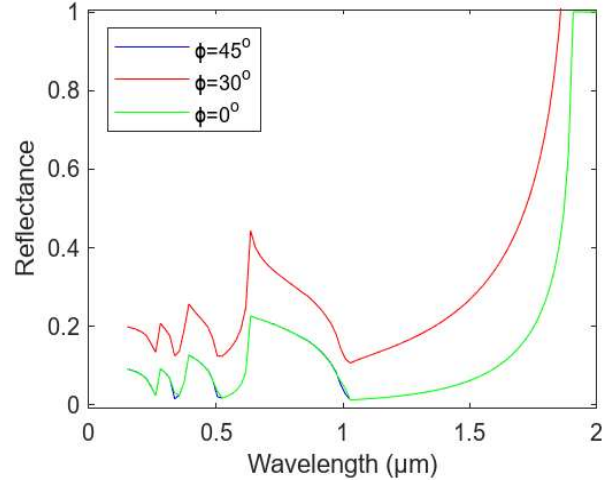

Fig. 17 Results of 2D calculation with $a = b = 0.95$ μm and $L_x = L_y = 1.0$ μm.

One issue to keep in mind is that the metal slabs or grids are infinitely deep, so all the transmitted light into the gaps will not be reflected. In reality, no systems can be infinitely deep, so some reflection from the bottom of the gaps will occur. Arbitrarily wide cells will minimize reflectance in my solution, but in actuality designing a broadband absorber with arbitrarily wide cells would increase substrate reflectance. These two competing factors must be balanced to achieve the lowest possible total reflection.

My solutions offer guidance for designing a broadband absorber. A periodic, cellular surface with thin walls has minimal area for specular reflectance. The x and y periodicity of the cells can be adjusted so that the wavelength reflected with the highest constructive interference (the first maximum below $\lambda = L$) from one direction's periodicity is a wavelength reflected with highly destructive interference (one of the minimums around $\lambda = L$) from the other direction's periodicity. As an example, Fig. 18 shows that light reflected from an $a = b = 0.95$ μm, $L_x = L_y = 1.0$ μm square grid experiences constructive interference at $\lambda = 637$ nm. Conversely, light reflected from an $a = b = 0.55$ μm, $L_x = L_y = 0.6$ μm square grid
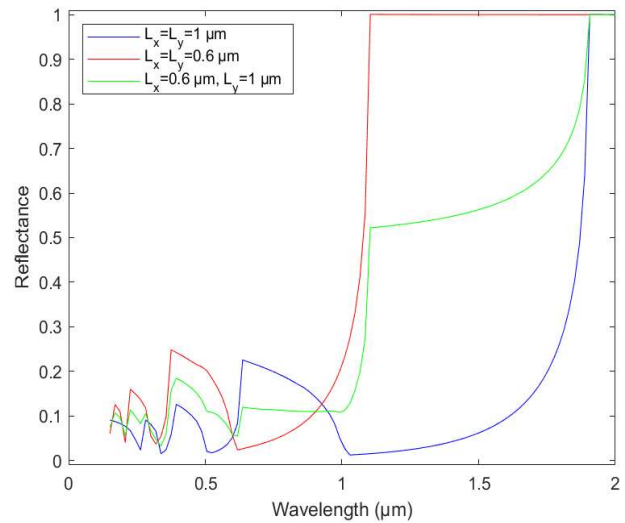

Fig. 18 Result of 2D calculation with metal thickness 0.05 μm and $\phi = 45°$. Appropriately combining multiple periodicities yields a broader region of low reflectance in wavelengths below 1.0 μm.

22

experiences destructive interference at that same wavelength. An $a = 0.55$ μm, $b = 0.95$ μm, $L_x = 0.6$ μm, $L_y = 1.0$ μm grid, which combines the two periodicities, has lower reflectance across a wider range of wavelengths.

4.2 A special case

If we fix a but expand b in Fig. 13, the walls of the grid in the y-direction will become smaller and smaller and eventually Fig. 13 will be identical to Fig. 9. Therefore, it is interesting to see how the 2D results discussed in Sec. 4.1 approach the 1D results discussed in Sec. 3.1. To be consistent with the grating conditions used in Sec. 3, I will consider the TE wave impinging on the interface with $\phi = 0$. As a result, $E_{ix} = H_{iy} = 0$ and the equations are significantly simplified. Assuming no E_x or H_y components are excited in the scattered or transmitted waves, $B_{mn} = 0$ for any m, n in Eq. (26) and only the D_{r0} coefficients are nonzero in Eq. (28). Under this condition, Eq. 28(b) dictates that the E_{yt} field has no y-dependance. Since boundary conditions require $E_{yt} = E_{ys}$, only the C_{m0} coefficients are nonzero in Eq. (26).

These greatly simplified equations can be solved using the technique outlined in Sec. 3. Reflectance results for the solution when $a = 0.95$ μm and $L_x = L_y = b = 1.0$ μm are shown in Fig. 19, alongside results from a 1D calculation with the same geometry and a calculation using the formalism of Sec. 4 with $\phi = 0$. That the three results are nearly identical verifies the validity of my methods and solutions.

When $\phi = 0°$ and $b = L_y$, Fig. 13 is exactly Fig. 9. When $b \lesssim L_y$, the grating is no longer uniform in the y-direction, but is instead divided by thin metal partitions. As b continues to decrease, we eventually arrive at the case of $\phi = 0°$ incidence on square, $b = a$, apertures (Fig. 17). The question then remains, what affect does this changing b have on the reflectance of an $E_x = 0$ wave?
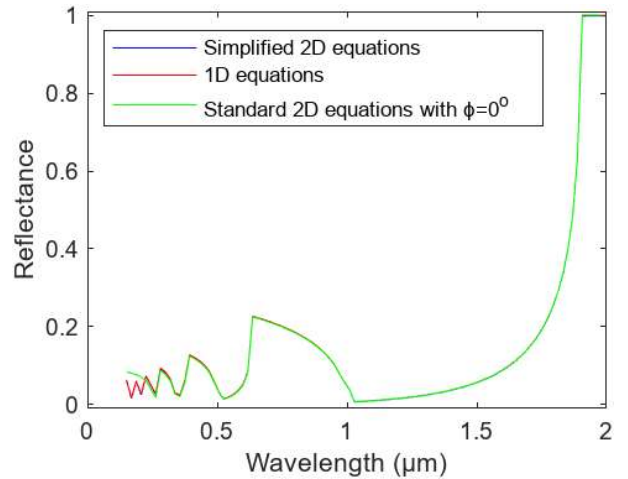

Fig. 19 Result of calculation using the methods of Sec. 4.2, Sec. 3, and Sec. 4 with $a = 0.95$ μm, $L_x = L_y = b = 1$ μm, and $\phi = 0°$.

Figures 20 and 21 demonstrate that the $b = L_y$ and the $b = a$ case have remarkably similar reflectance spectra when $E_x = 0$. Apparently, metal partitions in the x-z plane don't have a significant effect on an electric field polarized perpendicular to that plane. From the perspective of the boundary conditions dictated by Maxwell's equations, this makes sense. While the transverse components of $\vec{E}$ must be zero on a metallic interface, the normal component has no such restraint; charge accumulating on the surface of a conductor can generate a discontinuity in the normal component of the electric field. Thus, a wavelength-thin, perfectly conducting metal slab in the x-z plane should appear nearly transparent to the y-component of an electric field. Figure 21 has higher overall reflectance than Fig. 20 because the incident angle is glancing, a result consistent with Fig. 16 and fundamental reflectance theory.
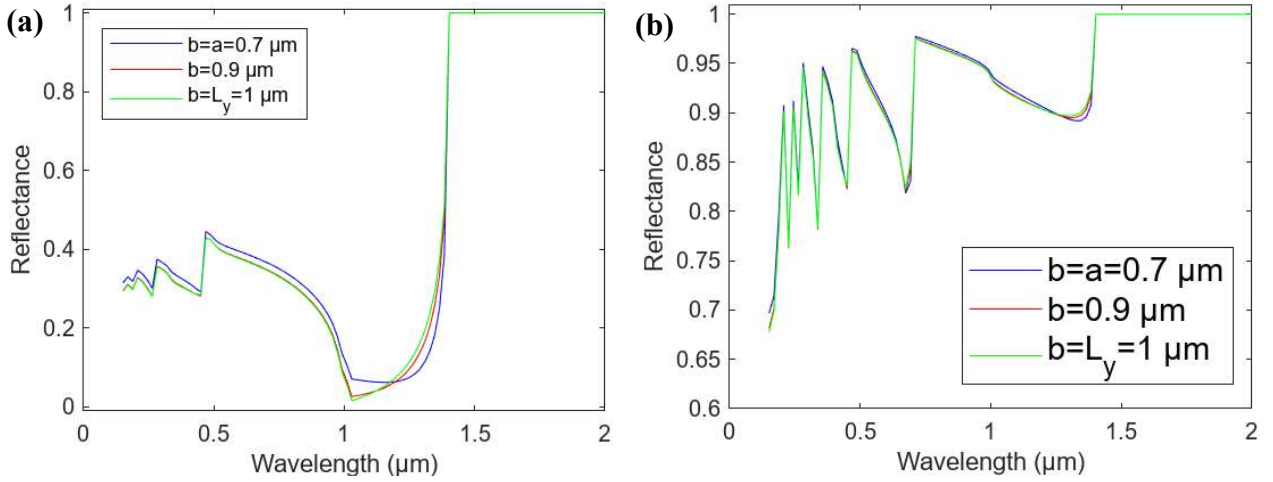
Fig. 20 Results of $E_x = 0$ calculation with $a = 0.7$ μm, $L_x = L_y = 1.0$ μm, and (a) $\theta = 1°$, (b) $\theta = 80°$.

5. Other geometries

The methods I've used can be extended to other geometries, such as circular apertures or aperiodic surfaces. To solve reflectance from an array of completely dark circular apertures, one can use the circular waveguide modes as the transmitted waves in the $z < 0$ region[16]

$$H_{zt} = \sum_{v,n=(0,1)}^{\infty} F_{vn} \sin(v\phi) J_v\left(\frac{\tau_{vn}\rho}{a}\right) e^{i\beta_{vn}z} \qquad (35)$$

where F_{vn} is the amplitude of the v, n mode; $J_v(x)$ is the Bessel function of the first kind of order v; τ_{vn} is the nth zero of $J_v(x)$; a is the radius of the waveguide; and $\beta_{vn} = \pm\sqrt{k^2 - \left(\frac{\tau_{vn}}{a}\right)^2}$. The other TE field components can be found using the Maxwell relations in Eqs. (27a)-(27c) and (29a)-

24

(29b). Then, apply boundary conditions at the $z = 0$ interface and solve for the mode amplitudes, as previously shown. The power can then be calculated using Eqs. (34a)-(34c).

Many of the dark surfaces found in nature and in the laboratory, such as ultradark butterfly wing patches and carbon nanotube forest crusts, are not perfectly periodic. What advantages are there to aperiodic surfaces over periodic ones, and how might my methods be extended to predict the reflective spectra of such materials?

Aperiodic structures could achieve lower overall reflectance over a wider wavelength range. As discussed in Sec. 4.1, structures with a constant, definite periodicity experience interference resonances that create large jumps and drops in reflectance, as seen in many of my 2D results. Structures with a periodicity that is different in the x-direction versus the y-direction experience less of these oscillations and exhibit a more-or-less smooth reflectance spectrum, as can be seen in Fig. 16. One might then hypothesize that aperiodic structures could have fewer to no resonances and a very smooth reflectance spectrum. That would be desirable for a broadband absorber.

Another consideration is the cutoff wavelength of aperiodic surfaces. My 2D results with square apertures have a sharp cutoff at $\lambda = 2a$, with reflectance rising quickly to 1 at $\lambda \lesssim 2a$. However, my results with rectangular apertures have a more gradual rise to the cutoff wavelength. Thus, one might expect that structures with random aperture shapes would experience a more gradual cutoff wavelength.

The question then, is how to parameterize and model a surface with randomized periodicity and aperture size. Consider a structure with an independent random variable distribution for each of the four parameters L_x, L_y, a, and b. If the standard deviation of these variables are small, we might call such a structure "quasi-periodic". One simple way to approximate the reflectance spectrum from this structure would be to form a linear combination of known, periodic reflectance spectra,

$$R(\lambda) = \sum_{L_x} \sum_{L_y} \sum_a \sum_b A_{L_x,L_y,a,b} R(L_x, L_y, a, b; \lambda) \tag{35}$$

where the coefficient A is the probability of a given aperture being of size $a \times b$ and having spacing L_x with its neighbors in the x direction and L_y with its neighbors in the y direction, normalized so that $\sum_{L_x} \sum_{L_y} \sum_a \sum_b A_{L_x,L_y,a,b} = 1$. If A is known, the spectra $R(L_x, L_y, a, b; \lambda)$ could be found using

the same methods as in Sec. 4. One can optimize the distributions of the physical parameters to achieve lowest $R(\lambda)$ across a wide wavelength spectrum.

6. Conclusions

The techniques that I have developed here can be used to find light scattering from a periodic or quasi-periodic, perfectly conducting, array of infinitely deep holes. Rather than using simulation, e.g. finite-element-time-domain (FDTD) methods, I solved Maxwell's equations numerically by applying mode-match boundary conditions between the incident, scattered and the transmitted waves at the interface. I assumed the transmitted waves to be modes of a perfect conducting waveguide. This has allowed me to directly observe the causes of structural color and what makes certain periodic and quasi-periodic materials dark. I have shown that interference is the primary factor in the wavelength dependence of reflectance from metallic metasurfaces. I have also shown how quasi-periodic materials can be dark over a wide spectrum of wavelengths by overlapping the constructive, bright interference due to certain periodicities with destructive, dark interference from other periodicities.

These solutions can be used to design a broadband absorber in the laboratory. For example, the issue of high infrared reflectance from carbon nanotube forests could be mitigated by growing the forests in a periodic or quasi-periodic cellular structure with thin walls and periodicity such that the infrared reflectance can be mitigated. A broadband absorbing material such as this would be useful for many applications including higher efficiency solar panels and thermoelectric devices.

Word count: 6012

Reflective writing

This project truly has served as the capstone of my undergraduate education. I have had to use my knowledge of mathematics, including complete, mutually orthogonal sets of functions; vector analysis; and probability theory, to develop the solution. The MATLAB platform has given me an opportunity to apply the programming skills I have gained from various computer science classes. Most critically, I have had to "think like a physicist" and combine mathematics, numerical methods, and an understanding of the physical reality and Maxwell's equations to tackle this problem.

My next goal is to earn a Ph.D. in optics and photonics, with the long-term goal of becoming a research scientist in the field. This Capstone experience has prepared me for that in many ways. Being a Ph.D. student is a delicate balance of coursework, reading papers, and conducting research. I presume that a professional researcher must balance the latter two as well as the other duties of his/her life. During the course of this capstone project, I have had to do exactly that. I have acquired time management and prioritization skills, including sticking to a daily, process-oriented schedule and regularly examining and refreshing my to-do list in light of my overarching end goal. These lessons will help me in every future endeavor, professional and otherwise. Additionally, the topic of my Capstone project is very relevant to my chosen field of study; the mathematics, physics, and even computer programming I have learned over the course of this project will benefit my future education and career.

Working with Dr. Shen has been a great opportunity for me to learn from and develop a relationship with an experienced mentor figure. I have learned how to communicate my ideas to him in a way that makes sense, as well as how to receive and act on communication from him. That includes mathematical ideas as well as feedback on my writings and presentations. While working with Dr. Shen, I have been able to get a close-up examination of how a professional physicist thinks and works through problems, which has been immensely insightful in helping me develop my own intuition. I have seen that nothing is easy, even for a professional, which has allowed me to be more patient with myself through difficulties, setbacks, and mistakes. Additionally, Dr. Shen knows the terrain of optics and photonics research much better than I do, and was able to point me towards interesting graduate programs and potential future mentors to

further my education after I depart USU. I wouldn't have known which schools were good to apply to without his direction.

The undergraduate physics curriculum basically focuses on four topics: classical mechanics, electromagnetism, thermodynamics, and quantum mechanics. This capstone project has allowed me to have an incredibly in-depth experience in electromagnetism, something I never could have gotten in a classroom. I have gained a greater understanding of Maxwell's equations and how to manipulate and interpret their results, for example, the boundary conditions used in my solutions. I can use the principles of Fourier theory and modal analysis almost in my sleep. I understand what it means to check my results with dimensional analysis and order-of-magnitude approximations, such as, "is the magnetic field smaller in amplitude than the electric field by the correct ratio?" These are all critical skills to have in physics. I have come to understand, from my own experience, what it means to say that the more you know about a topic, the more interesting it becomes.

Along, the way, the journey has been anything but easy. At the beginning of my project, I was used to learning through lectures and notetaking in a classroom, but it quickly became apparent to me that learning through a literature review is a very different challenge. Once I learned how to parse the handful of graduate-level textbooks and professional papers Dr. Shen gave me to start with, I had to learn how to find additional resources on my own, determine whether or not they were interesting and relevant to my work, and then read them for understanding. For me, this was among the most difficult parts of my Capstone project, but I feel it will also be among the most important lessons I am still learning as I go forward as a researcher.

Before beginning my Capstone project, I had taken some introductory computer science classes, so gratefully I didn't have to build my knowledge of coding entirely from the ground up. However, I had never coded in MATLAB before, so that presented a new opportunity for me to learn and grow my skills. Additionally, the problems introduced in basic computer science coursework are very different from the problems we need to solve in physics. I learned how to blend my knowledge of mathematics and programming to write something that was both elegant and, eventually, correct. The critical word there is "eventually", because it took many, many hours of debugging, talking to myself, and combing through my code line by line before it actually

worked. All that, however, I can accept now as an important lesson in patience and an initiation that every computational physicist must pass through over and over again.

During the course of this project, I've learned how to use many resources that are used by researchers across every discipline. Perhaps foremost among those is the citation manager Zotero. That program saved me so many headaches and I will laud its praises until the end of time. As I mentioned previously, I also learned how to write code in MATLAB, which is a very common language among engineers, but less so among physicists. Since my graduate degree program is in an engineering department, MATLAB knowledge will very likely be a handy skill to have in my future. On a similar note, I have also had to learn a lot of computational math skills during my Capstone project, such as error propagation, numerical stability, and vectorization of array operations. I have never formally taken a computational math course, but through my research I have gained many of the basic proficiencies of the field. Because I learned these skills via my own mistake-ridden experience, I will remember them longer than if I had just learned it in the classroom.

Finally, this Capstone research experience has given me the ability to aid in the education of other future researchers. I might call them the "next generation", but in reality, these young researchers are only a year or two behind me. As I have tried to pass on the knowledge I have gained, I have been able to grow my appreciation for how much this Capstone project has truly taught me. I've grown proficient in many areas of mathematics, computer science, and physics that will be important to me as I continue my studies and future research. I have learned important lessons about priorities, time management, and science communication. And, since I am not too far away from the students I have trained to carry on after I graduate, I have been able to share what I have learned in a way that perhaps is more meaningful and understandable. For all of these many reasons, I am grateful to have had this Capstone experience.

Word count: 1201

Bibliography

[1] E. Hecht, *Optics*, 5 ed (Pearson Education, Inc, Boston, 2017).

[2] D.J. Griffiths, *Introduction to Electrodynamics*, Fourth edition (Pearson, Boston, 2013).

[3] H.A. Lorentz, *The Theory of Electrons and Its Applications to the Phenomena of Light and Radiant Heat*, Dover ed (Dover Publications, New York, 1952).

[4] "MIT OpenCourseWare | Architecture | 4.492 Daylighting, Fall 2004 | Home," (n.d.).

[5] A.A.G. Amer, S.Z. Sapuan, N. Nasimuddin, A. Alphones, and N.B. Zinal, "A Comprehensive Review of Metasurface Structures Suitable for RF Energy Harvesting," IEEE Access **8**, 76433–76452 (2020).

[6] A.S. Rana, M. Zubair, Y. Chen, Z. Wang, J. Deng, M.T.S. Chani, A. Danner, J. Teng, and M.Q. Mehmood, "Broadband solar absorption by chromium metasurface for highly efficient solar thermophotovoltaic systems," Renew. Sustain. Energy Rev. **171**, 113005 (2023).

[7] T. Deng, J. Liang, T. Cai, C. Wang, X. Wang, J. Lou, Z. Du, and D. Wang, "Ultra-thin and broadband surface wave meta-absorber," Opt. Express **29**(12), 19193–19201 (2021).

[8] J. Hu, S. Bandyopadhyay, Y. Liu, and L. Shao, "A Review on Metasurface: From Principle to Smart Metadevices," Front. Phys. **8**, (2021).

[9] D.G. Stavenga, "Thin Film and Multilayer Optics Cause Structural Colors of Many Insects and Birds," Mater. Today Proc. **1**, 109–121 (2014).

[10] A.L. Davis, H.F. Nijhout, and S. Johnsen, "Diverse nanostructures underlie thin ultra-black scales in butterflies," Nat. Commun. **11**(1), 1294 (2020).

[11] R.H. Siddique, Y.J. Donie, G. Gomard, S. Yalamanchili, T. Merdzhanova, U. Lemmer, and H. Hölscher, "Bioinspired phase-separated disordered nanostructures for thin photovoltaic absorbers," Sci. Adv. **3**(10), e1700232 (2017).

[12] K. Cui, and B.L. Wardle, "Breakdown of Native Oxide Enables Multifunctional, Free-Form Carbon Nanotube–Metal Hierarchical Architectures," ACS Appl. Mater. Interfaces **11**(38), 35212–35220 (2019).

[13] B.D. Wood, J.S. Dyer, V.A. Thurgood, N.A. Tomlin, J.H. Lehman, and T.-C. Shen, "Optical reflection and absorption of carbon nanotube forest films on substrates," J. Appl. Phys. **118**(1), 013106 (2015).

[14] C.M. Lange, and T.-C. Shen, "Fabrication of height-modulated carbon nanotube forests: Morphologies and prospects for broadband absorption," Carbon Trends **4**, 100070 (2021).

[15] A. Ishimaru, *Electromagnetic Wave Propagation, Radiation, and Scattering: From Fundamentals to Applications* (John Wiley & Sons, Inc., Hoboken, NJ, USA, 2017).

[16] D.M. Pozar, *Microwave Engineering*, Fourth Edition (Addison-Wesley, 1990).

Author bio

Wesley Mills grew up in Clovis, California, but decided to return to his family's Cache Valley roots and attend Utah State University. While attending university, he has participated actively in undergraduate research through the Peak Summer Research Fellowship, USU Undergraduate Research Fellowship, and USU Honors Department. He was also the recipient of a 2022 Goldwater Scholar award. In May 2023 he will graduate Summa Cum Laude with a Bachelor's Degree in physics. He and his wife will then flee the snow and return to California, where he has been accepted into the electrical engineering Ph.D. program at UC Santa Barbara.